Experimental and numerical investigations of thermal characteristics of heat exchangers in oscillatory flow

Olusegun M. Ilori[a,b], Artur J. Jaworski[c], Xiaoan Mao[a]

[a] Faculty of Engineering, University of Leeds, Leeds LS2 9JT, United Kingdom

[b] R&D Department, Airedale International Air Conditioning Ltd, Leeds Rawdon, Leeds, LS19 6JY, United Kingdom

[c] School of Computing and Engineering, University of Huddersfield, Huddersfield, HD1 3DH, United Kingdom.

Abstract

Heat exchangers under oscillatory flow conditions constitute a critical component of thermoacoustic engines and coolers for which effective design methodologies are not yet available. In this study, the thermal and pressure drop performance of compact Tube Heat Exchanger (T-HEX) under oscillatory flow conditions is investigated using experimental and numerical methods. A standing wave experimental set-up, driven by the Qdrive linear alternator, and a measurement technique were developed to measure the temperature and acoustic pressure near the T-HEX simultaneously. The symmetric arrangement of three identical heat exchangers, one 'hot' heat exchanger, centrally placed between two 'cold' heat exchangers, is employed for an improved thermal analysis. Furthermore, aerodynamic shape is used on the heat exchangers gas channels to improve flow conditions associated with a sudden change in the cross-section. Experimental results are found to agree well with the predictions from three-dimensional Computational Fluid Dynamics (CFD) models. The Nusselt number and pressure drop due to minor losses show dependency on the drive ratio (measured maximum oscillating pressure to the system mean pressure), the edge shape and hot heat exchanger temperature.

At a high amplitude, the edge shape significantly minimises the minor loss pressure difference, with negligible effect on the thermal performance. The results reported in this study will benefit the development of compact heat exchangers for the thermoacoustic engines/refrigerators or Sterling engines/coolers in cryogenic applications.

1. Introduction

For the development of thermoacoustic engines and coolers with high performance, an optimum design for the heat exchanger is an essential requirement. A typical thermoacoustic system employs oscillatory flow as a means of energy transfer within its internal elements (heat exchangers, stack or regenerator) to produce acoustic power (engine) or consume it for heat pumping (cooler). Either in thermoacoustic engine or cooler, heat exchangers act as a heat source and heat sink, which implies that the efficiency of the device can be improved through an optimised heat exchanger design. A detailed description of the fundamental of energy transfer and the Sterling-like thermoacoustic cycle that is responsible for thermoacoustic effect in the heat exchange components of thermoacoustic systems has been described by Swift [30,31].

The two primary design considerations for a heat exchanger in oscillatory flow are to maximise heat transfer for relatively short acoustic displacement of the oscillating gas and to minimise pressure losses. Both considerations depend on flow conditions and suggest that the geometric design of a heat exchanger can affect its thermal and minor loss pressure drop performance. Unlike the heat exchangers in steady flow which has well-established design guidelines, the presence of acoustically induced flow and the cyclic flow reversal at certain distances in energy system such as thermoacoustic devices, implies that the heat transfer cannot arbitrarily be increased by increasing the heat transfer area of the heat exchanger [9]. This makes the design and optimisation of heat exchangers in oscillatory flow a challenging task, which forms the basis for the lack of effective oscillatory flow design methodologies.

In the design of heat exchangers in oscillatory flow, the commonly used methods include the quasi-steady approximations such as the well-known TASFE (Time-Average Steady-Flow Equivalent) [28] and RMS-Re (Root Mean Square Reynolds Number), which are based on heat transfer correlation from steady flow conditions. However, it has been reported [21,26] that these approximations did not hold at higher oscillating velocities which result in over-prediction of heat transfer as well as under-prediction of the minor losses [20]. Also, the heat transfer model based on boundary layer conduction over predicts heat transfer in oscillatory flow [44]. Therefore, the design and development of heat exchangers in oscillatory flow would require further study to achieve a more reliable performance data for establishing detailed design guidelines.

Research works have been carried out to study the thermal performance of heat exchangers in oscillatory flow. Finned type heat exchangers [13,23,32,33], parallel plate type [29,38], and parallel tube types [21] have been studied to determine the influence of normalised displacement amplitude, fin or plate spacing, plate thickness, and acoustic Reynolds number (based on the peak acoustic velocity between tubes), on the heat transfer performance of heat exchangers. These studies have used either a single ambient or cold heat exchanger for heat transfer performance characterisation or a pair of adjacent 'cold' and 'hot' heat exchangers (with or without gap) in an attempt to improve the heat transfer estimation and to propose oscillatory flow correlations. However, the issue of heat leak through the working fluid to the surrounding could not be resolved entirely because of lack of symmetry in the heat exchanger arrangement. This suggests that the heat transfer estimation in oscillatory flow can still be improved by using a symmetric arrangement of heat exchangers, to arrive at a more accurate design guidelines for the oscillatory flow heat exchangers.

The edge shape of a heat exchanger is of high importance in thermoacoustics and can be explored for an optimum design that is capable of minimising the minor losses associated with a change in cross-section of the gas channels, which often translate into a nonlinear acoustic impedance that can diminish the efficiency of the system [10,24,45], thereby contributing to the overall system efficiency. It is interesting to know that the studies above considered heat transfer and fluid flow conditions through square-edged geometries, which often produce disturbances that may generate minor losses and impact

pressure drop performance negatively. In thermoacoustic engines and coolers, heat exchangers are placed near to the stack/regenerator with a small separation gap, and it would appear reasonable that this arrangement may alter the nonlinear impedances of the heat exchangers by reducing jetting and vortex formation and shedding. On the other hand, if the flow is modified, for example by using aerodynamic edge shape, in such a way to mitigate these non-linear effects, there may be a corresponding effect on the heat transfer. The works of Smith and Swift [31,46] focused on the experimental investigation of the effect of rounded edge on flow ducts against parametric operating conditions, but no heat exchanger was investigated and it unclear what the effect of edge shape will be on the heat transfer and pressure drop performance. Therefore, the extent of geometric effect on the performance of a heat exchanger in oscillatory flow needs to be considered, and it is one of the objectives of this paper.

Another important area in the study of heat transfer in oscillatory flow is the determination of heat transfer coefficient on the gas side of the heat exchanger. In oscillatory flow, the fluid temperature changes in time and location due to the forward and backward movement of the gas particles, which in turn dictate different heat transfer behaviour to that of steady flow. Currently, there appears to be no consensus in the literature over the definition of the heat transfer coefficients in the oscillatory flow, which has been defined to be application dependent in the relevant research studies [5,29,41].

To understand the heat transfer phenomenon in oscillatory, it may be worthwhile to investigate the fundamental features of the velocity and temperature fields that show the flow behaviour and how it affects the heat transfer performance of the heat exchangers. Several methods have been used for this purpose including the Particle Image Velocimetry (PIV) [1] and Planar Laser Induced Fluorescence (PLIF) [29], numerical simulations [18,39] and combination of techniques [40]. These methods provide useful information, in two-dimension, for the understanding of flow physics in a parallel plate structure under oscillatory flow. However, the information about the three-dimensional (3D) effects [31] which are present for the compact heat exchangers still requires further investigation. A 3D CFD model offers the advantage of providing useful information that can complement the experimental data to give an understanding of the heat transfer and flow physics inside the heat exchangers in oscillatory flow. In

4

the CFD technique to modelling of thermoacoustic engines and refrigerators [22,42,43], the internal elements are often accounted for by using porous media method, where a volume porosity is used to account for the solid fraction, and the pressure loss of the heat exchanger is evaluated using the steady flow relation [14,35]. While this approach reduces the computational effort for modelling the whole thermoacoustic device, it does not give information about the contribution of each constituent element of the system such as the thermal interaction of working fluid with the thermal contact area of the heat exchangers. Therefore, modelling the actual configuration of the heat exchanger will provide more interesting information on nonlinear phenomena like turbulence, streaming and vortex shedding, which is required for the design needs, but cannot be captured with the existing classic linear theory or the simplified geometries.

This paper focuses on the investigation of the heat transfer, and pressure drop due to minor losses in the Tube-Heat Exchangers (T-HEX) under oscillatory flow, using experimental and numerical methods. In the experimental aspect, a purpose-built setup and measurement techniques are specifically developed to test the heat exchangers (without a stack or regenerator) under high pressure and oscillatory flow conditions as relevant to thermoacoustic systems. In the numerical aspect, 3D CFD models are developed and validated based on the same geometric dimensions of the T-HEX and the measurement data in the experiments. Comparison between experimental and simulation results are first carried out. Further analyses are then performed with the simulation results to extend the understanding of the thermal-fluid processes in oscillatory flow. The investigations are carried out by examining the effect of geometry (edge shape), drive ratio (measured maximum oscillating pressure and the system's mean pressure) and temperature of the hot heat exchanger. These effects are considered in the pressure amplitude distribution, averaged temperature, velocity amplitude and flow structure, heat fluxes, Nusselt number, and the pressure drop due to minor losses.

The significance of this study includes the use of a symmetric arrangement of heat exchangers to improve the heat transfer estimation on a T-HEX. Also, an aerodynamic edge-shape is used on the T-HEX (ogive) gas channel, to modify the flow condition and minimise the pressure drop due to minor losses, with negligible effect on the heat transfer performance. This study offers the development of

5

measurement technique to simultaneously measure the temperature and the acoustic pressure within a high-pressure environment, which is essential for a well-defined condition in the study of heat exchangers in oscillatory flow. It is anticipated that the results here will contribute to the development of the design guidelines for the heat exchangers of the next generation of thermoacoustic engines/refrigerators or Sterling engines/coolers in cryogenic applications.

2. Experimental methods

Fig. 1 shows the overview of the half-wavelength standing wave experimental setup and the measurement technique in this study. The rig is designed and constructed as a test facility for investigating the thermal and hydraulic performance of heat exchangers (without the stack or regenerator) in oscillatory flow, as relevant to the conditions in practical thermoacoustic engines and refrigerators. The setup is 8.9m long and consists of an acoustic driver (Q-drive-1S102D), test section enclosing three T-HEX arranged in series (a hot heat exchanger centrally placed between two cold heat exchangers), 2-inch circular cross-sectional resonator, gas-charging unit, hot and cold water loops, measurement devices and data acquisition system. Helium gas is used as the working fluid in the set-up, which has a total volume of 21 L at 1 bar mean pressure. The experimental rig is operated at the resonance frequency (f) of 53.6 Hz.

2.1. Acoustic driver

An essential requirement in this study is to test the T-HEX sets in an oscillatory flow which is generated and sustained in the setup using a Qdrive acoustic driver (1S102D). The acoustic power output from the driver is 225W at the maximum piston displacement of 12mm (peak to peak), and it is powered and controlled (frequency and excitation voltage) by a power supply, Allen-Bradley model PowerFlex700, and housed in a pressure vessel that allows connection to the rest of the test rig via a flanged 2-in. 90° elbow that matches the flanged 2-inch straight resonator. The peak to peak piston stroke of the driver was monitored using Laser Displacement Sensor (LDS) LK G152 (0.25 V/mm (4 mm/V)) with a measurement range of±10.8 V, positioned directly above the optical window in the acoustic driver

housing. The resonator defines the phase of pressure and velocity of the oscillating helium gas that interacts with the boundaries of the three T-HEX in the test section.

2.2. Test section and heat exchangers

The test section houses the cross-flow T-HEXs, spacers, dynamic pressure transducers, Type-K thermocouples (T/C) and the insulation materials (silicate wool), while its lid accommodates the feedthrough assembly for T/C's and Swagelok fittings for transducers' cables and water tubes (cf. Fig. 1). The test section is fabricated from a SCH40 SS-316 material, and its mid-point is located at a distance x=4.29m from the pressure antinode (x=0). The three identical T-HEXs are arranged in series (two cold heat exchangers 'CHX1 and CHX2' and a hot heat exchanger 'HHX') to form a 'core' that is enclosed within the high pressure environment. The geometric parameters of the T-HEX are shown in Table 1, and the two configurations that are investigated here are identified as T-HEX (flat) and T-HEX (ogive) as shown in Fig. 2. THEX (flat) (Fig. 2a) is the T-HEX with a squared edge having curvature radius (RC) of 0 mm, and the T-HEX (ogive) (Fig. 2b) is the T-HEX with aerodynamic shape (ogive) having RC of 7 mm. An 'ogive' edge shape was selected for use in this study based on the knowledge of using streamlined shape to reduce drag at the boundary layer, thus minimising pressure drop [11].

The T-HEX are designed as water heated and water cooled compact heat exchangers, which are fabricated from a block of aluminium material that has a thermal conductivity of 180 W/m·K. On the gas side of the T-HEX, 89 circular channels 'tubes' are arranged in a triangular pitch pattern (Isosceles triangle) with 4mm and 5.5mm horizontal and vertical distances. Pressurised helium gas oscillates through the tubes and water flows uni-directionally through the ten rectangular channels (12mm×1.5mm×67mm each) at atmospheric pressure in a crossflow pattern. Each T-HEX is clamped between two end-caps to allow connection to the water tubes. During the experiments, a refrigerated circulator with cooling power of 500W (at 20 °C) is used to maintain the inlet temperature of the CHX1 and CHX2 at a constant temperature of 10 °C. A PID temperature controller (Omega Model CN8592) is used to control the temperature of the hot water bath within±1 °C accuracy at a desired HHX inlet

temperature (30, 50 and 70 °C). A constant flow rate of 0.44 L/min is used on all the heat exchangers, and it is achieved by Swagelok needle valve and measured by a mini flow turbine with an accuracy of 0.005 L/min.

The T-HEXs are separated using four spacers to minimise the heat conduction between the heat exchangers. Two middle spacers separate the CHX1, HHX, and CHX2 with an equal gap of 4 mm, while two end spacers connect the CHX1 and CHX2 to the steel resonator. Each spacer is fabricated from Nylon 6 material (0.88 W/m·K at 25 °C) to an inner radius of 57.4mm and a thickness of 8.8 mm. Customised fittings for the dynamic pressure sensors and the T/C's are mounted through the spacers to facilitate simultaneous measurement of oscillating pressure and mean temperature near the heat exchangers. Pressure sensors are flush mounted (cf. Fig. 1) at 6.5mm from the nearest T-HEX. Details of the operating parameters and the gas properties in the experiment and simulation are shown in Table 2.

2.3. Measurements

On the gas side in the setup, 20-pair of 0.5mm diameter Type-K thermocouples (T/C's) are positioned in the high-pressure environment using a high-density feedthrough assembly (cf. Fig. 1. Three T/C's are positioned near the heat exchangers at x=3.44 m, 3.84, 4.04 and 4.74 m, to measure the gas temperature, which implies that 12 T/C's (T1–T12) are used for the gas temperature measurement around the heat exchangers. An average of three temperature readings at each location is utilised in the heat transfer calculations. T13, T14 and T15 are attached to the wall of the heat exchanger gas channels to measure the surface temperature directly, which are also employed as boundary conditions in the simulation. Additional thermocouple T16 and T17 are used to monitor the gas temperature at distance 202mm from the CHX1 side and inside the insulation material, respectively, to observe the heat transfer by conduction through helium gas and the insulation material. T18–T23 are T/C Type K-310 of 1.0mm diameter, installed in the water tubes (cf. Fig. 1b) to obtain temperature data from the water side. Also, T24 is used to monitor the temperature of the resonator to determine the heat loss through the resonator wall.

8

Several dynamic pressure transducers (P0–P7) from PCB PIEZOTRONICS (model 112A22) are distributed along the experimental rig to measure the acoustic pressure at different locations. P0 is positioned at the pressure antinode (x=0) in the standing wave at the closed end in the rig. The pressure amplitude from P0 is used as the controlling parameter during the experiments and for determining the resonance frequency, i.e. the operating frequency at which the highest acoustic pressure was achieved. P1, P2, P3 and P7 are located at distances x=3.44 m, 3.84, 4.04 and 4.74 m, respectively, from the closed end. At some point, port of P3 was used interchangeably between a pressure transducer and a thermocouple. The acoustic pressure measurements from P2 and P7 are used as the acoustic boundary conditions in the simulation. The pressure amplitudes near the T-HEX are measured using P4, P5 and P6, which are installed at 32mm apart in the high pressure environment without exposing the sensors to the pressurised helium gas. The signal cables from P4, P5 and P6 are channelled through stainless tubes of 8mm diameter each and the feedthrough fittings. The signal outputs (volt) from the pressure transducers are amplified using ICP signal conditional (model 482C16). All readings (temperature, pressure, piston displacement, and water flow rates) from the sensors are transferred to the PC via data acquisition card (OMBDaq Temp Model 14) from Omega. The pressure and displacement signals are acquired simultaneously and transformed through FFT to find the individual phases and the phase difference, which are obtained from LABVIEW programme with an accuracy of 0.01°.

The data collection procedure during the experiments usually starts by allowing the two water loops to first create heating and cooling loads in a typical set of heat exchangers. When the system is in a thermal equilibrium condition, the acoustic driver is switched on to excite the flow and cause the compressed helium gas within the set-up to oscillate through the heat exchangers, thereby generating the transfer of heat between the hot and cold heat exchangers. Simultaneously, oscillating pressures are produced as the helium gas moved through the heat exchangers. When the system reaches steady oscillatory and thermal conditions, temperature and pressure amplitude data from thermocouple and pressure transducers are recorded on the gas side at every location within the test section. Similarly, for the water side, water temperatures and flow rate data are recorded. A similar procedure is involved for completing all experiments on each set of heat exchangers and edge shapes.

2.4. Data reduction

The measured temperatures and pressure amplitudes from the experiments are used in the heat transfer and pressure drop calculations. The heat transfer rate ($\dot{Q}$) can be calculated from:

$$\dot{Q}_h = \rho_w q_v c_{p,w} (T_{w,i} - T_{w,o})_h$$
$$\dot{Q}_{c1,c2} = \rho_w q_v c_{p,w} (T_{w,o} - T_{w,i})_{c1,c2} \tag{1}$$

where ρ_w, q_v and c_p, are the water density [47], volume flow rate and specific heat capacity [48], of water, evaluated using the average of water inlet and outlet temperatures $(T_{w,in} + T_{w,out})/2$. The heat loss ($\dot{Q}_{loss}$) in the experiment is evaluated to ensure the accuracy of the heat transfer calculations. Before every experiment, a static measurement (i.e. no flow excitation) was conducted to evaluate heat loss by conduction, when the system is in a thermal equilibrium condition. The heat transferred to or removed from the gas is evaluated using the temperature difference between the water inlet and outlet of each heat exchangers, which is attributed to the heat transfer by conduction since there was no flow excitation. The maximum of these values is 15.59, 29.19 and 17.17W for CHX1, HHX, and CHX2, respectively, at HHX inlet temperature (T_h) of 70 °C and CHX1 and CHX2 inlet temperatures ($T_{c1,c2}$) of 10 °C. Also, heat loss through the insulation material is evaluated using Fourier equation, $\dot{Q}_{loss} = k_{ins} A_{hx} (\Delta T_{ins}/\Delta x)$, where k_{ins}, A_{hx}, ΔT_{ins} and Δx are the thermal conductivity of insulation, HEX outer surface area, temperature difference and the thickness of insulation. Additional heat loss through helium gas is also monitored at a distance 202mm from CHX1 (cf. Fig. 1. The heat transfer rates through the insulation material and the helium gas are 102.4mW and 14 mW, respectively (at $T_{c1,c2}$=10 °C and T_h=70 °C). During the heat transfer analysis, the estimated heat leaks are subtracted from the heat transfer rates. Other sources of heat leak include the heat conduction through the fittings. However, this is difficult to account for and considered negligible in this study.

The convective heat transfer coefficient, h, on the gas side of the heat exchangers are determined as [7,32]:

$$h_{h,c1,c2} = \frac{\dot{Q}_{h,c1,c2}}{A_s \left[T_s - \left(\frac{T_{g,in} + T_{g,out}}{2} \right) \right]}$$

(2)

where $\dot{Q}$, $(T_{g,in} + T_{g,out})/2 = T_i$ is the heat transfer rates, $T_{g,in}$ and $T_{g,out}$ are the gas temperatures at the inlet and outlet of the heat exchangers gas channel. T_i is the mean gas temperatures at the locations near the heat exchangers (cf. Fig. 1). T_s is the measured surface temperature of the gas channel. Subscripts h, c1, and c2 denote the heat transfer conditions for the HHX, CHX1 and CHX2. The expression in the square bracket in Eq. (2) is often referred to as the thermal potential for the heat transfer coefficient. In oscillatory flow, the thermal potential is application dependent [5,29,41] and it is defined here to reflect the contribution of the gas temperatures at the inlet and outlet vicinity of the T-HEX gas channel. The Nusselt number (Nu) is related to the heat transfer coefficient (h) in the following expression as:

$$Nu_{h,c1,c2} = \frac{h d_h}{k}$$

(3)

where d_h is the hydraulic diameter.

The drive ratio (DR) constitutes a parameter by which the intensity of thermoacoustic oscillations is evaluated in practical thermoacoustic systems [25,31,36] and is described by:

$$DR = \frac{|p_0|}{p_m} \times 100\%$$

(4)

In the experiments, the DR is controlled by varying the excitation voltage that is supplied to the acoustic driver at a fixed mean pressure and resonance frequency, which in turn changes the gas parcel displacement amplitude (ξ_1) accordingly. The ξ_1 can be converted to acoustic velocity (u_1) and vice versa using $\xi_1 = |u_1|/\omega$, with the velocity leading the displacement by 90° in phase. Therefore, the relationship between the DR and ξ_1, for an ideal gas behaviour, can be expressed as [31]:

11

$$\xi_1 = \frac{aDR}{\omega}\sin(k'x) \tag{5}$$

where a, ω, k', and x are the speed of sound, angular frequency, angular wave number, and the distance (in the direction of wave propagation) from the pressure anti-node (x=0). Other important parameters that influence the heat transfer are the thermal (δ_κ) and viscous (δ_v) penetration depths which are defined as:

$$\delta_\kappa = \sqrt{\frac{2k}{\omega\rho c_p}}, \delta_v = \sqrt{\frac{2\mu}{\omega\rho}} \tag{6}$$

where k, μ, ρ and c_p are the thermal conductivity, dynamic viscosity, the density and specific heat capacity of helium gas. The thermal and viscous penetration depths are 0.46–0.56 mm and 0.38–0.46 mm, respectively, for the range of operating temperatures in the experiments and the simulation (10–150 °C). The Prandtl number can be expressed as Pr = $(\delta_v/\delta_\kappa)^2$ = $\mu c_p/k$, which gives a value of approximately 0.68 at an average value of the penetration depths. The acoustic Reynolds number is defined based on hydraulic diameter as:

$$Re_1 = \frac{\rho u_{m,h} d_h}{\mu} \tag{7}$$

where um,h is the velocity amplitude at the centre of the HHX (x=4.29m), obtained from $u_{m,h} = u_1/\sigma$, where σ is porosity of the heat exchanger defined as $\sigma = A_o/A_{fr}$. A_o and A_{fr} are the cross-sectional area of the gas flow channel and the total frontal core area of the heat exchangers, respectively [33,38]. The temperature-dependent thermal conductivity (k) and viscosity (μ) of helium are evaluated as [31]:

$$k = 0.152\left(\frac{T}{T_0}\right)^{0.72}, \mu = 1.99 \times 10^{-5}\left(\frac{T}{T_0}\right)^{0.68} \tag{8}$$

The density is defined following an ideal gas law as, $\rho_m = P_m/RT$, where R is the specific gas constant. Following Swift [31] and Marx et al. (2004), the pressure drop due to minor losses in oscillatory flow is defined as:

$$\Delta P = \frac{1}{2}K\rho_m u_1^2 \tag{6}$$

where K is the minor loss coefficient, which has been shown to depend on the flow direction within an acoustic flow cycle [8,20].

The measurement uncertainty in the experimental result is evaluated based on the approach described in the literature [2,6,17]. The temperatures on both the gas and water sides of the heat exchangers are measured with a relative uncertainty of 0.2 °C. The error bars on the heat flux and Nusselt number calculations, as will be discussed later, are determined based on this method and represent combined uncertainties of 12.5% and 12.6%, respectively. The uncertainties from the geometric tolerance of the heat exchanger fabrication and thermal conductivity of helium are assumed negligible.

3. Numerical methods

3.1. Model description and methodology

The 3D models of the T-HEX (flat) and T-HEX (ogive) are developed in ANSYS Fluent 17.0 [3]. Fig. 3 shows the method of integrating the experiments with the CFD model. The modelling phase begins with the development of a 2D model [12] based on the data from the literature. From this 2D model, it was established that the computational domain of 0.9m is sufficiently long to prevent the influence of the upstream and downstream flow conditions on the flow structures near the heat exchangers. Subsequently, the experimental set-up is developed, and data are collected, which are then used for the boundary and initial conditions and the result validation.

3.2. Computational domain and solution procedure

The inlet (x=3.84 m) and outlet (x=4.74 m) of the 0.9m computational domain, as shown in Fig. 4a, correspond to the locations of P2 and P7 in the experimental set-up (cf. Fig. 1). For meshing purposes, the domain is decomposed into three segments, consisting of the HEXcore, the upstream and the downstream sections. Fig. 4b and c show the unstructured mesh in the HEX-core and the structured mesh in the other sections. Fig. 5 shows the general procedure for achieving the simulation results. The ovals and boxes in the middle of the flow chart represent the main workflow within the solver. Calculations start at an assigned time step size (Δt), which must be chosen small enough to achieve the desired accuracy and avoid numerical divergence. The Δt is defined as:

$$\Delta t = \frac{1}{Nf} \tag{10}$$

where N is the number of time steps over one flow cycle, which is found to be 600 after the sensitivity check on the time discretisation. The mesh quality is assessed through the maximum skewness, minimum orthogonal quality and aspect ratio, with values of 0.7, 0.3, and 22.1, respectively, which are well within the acceptable range [3] and allowed the simulation results to converge based on the chosen criteria, as discussed in the next section.

3.3. Physical model

The unsteady flow fields are solved using 3D Navier-Stokes equations [3,37]. Buoyancy effect is considered in the simulation, and the Reynolds-Averaged Navier-Stokes (RANS) equation is used for the turbulence model closure. Previous relevant studies [18,19] have used RANS equations to model turbulent flow through the heat exchangers in oscillatory flow. The RANS equations are derived from Navier-Stokes equations by time averaging the transport and energy equations, with variables decomposed into mean and fluctuating components, $\varphi = \bar{\varphi} + \varphi'$, where $\bar{\varphi}$ and φ' are the mean and fluctuating components of the scalar variable such as velocity, and pressure. In conservative form, the RANS equations can be written for the continuity, momentum and energy equations as:

14

$$\frac{\partial \rho}{\partial t} + \frac{\partial}{\partial x_j}(\rho u_i) = 0 \tag{11}$$

$$\frac{\partial(\rho u_i)}{\partial t} + \frac{\partial(\rho u_i u_j)}{\partial x_j}$$

$$= -\frac{\partial p}{\partial x_i} + F_i + \frac{\partial}{\partial x_j}(\tau_{uj})_{\text{eff}} + \frac{\partial}{\partial x_j}(-\overline{\rho u_\iota' u_J'}) + \frac{\partial}{\partial x_i}(-\overline{\rho u_\iota'^2}) + S_m \tag{12}$$

$$\frac{\partial}{\partial t}(\rho E) + \frac{\partial}{\partial x_i}[u_i(\rho E + p)] = \frac{\partial}{\partial x_j}\left(k_{\text{eff}}\frac{\partial T}{\partial x_j} + u_i(\tau_{uj})_{\text{eff}}\right) + S_h \tag{13}$$

where F, S_m and S_h are the external force, and source terms. $(\tau_{uj})_{\text{eff}}$ and $-\overline{\rho u_\iota' u_J'}$ are the effective stress tensor, and Reynolds Stresses term used to model momentum equation for the turbulence affected flow, and they are defined as:

$$(\tau_{uj})_{\text{eff}} = \mu\left(\frac{\partial u_j}{\partial x_i} + \frac{\partial u_i}{\partial x_j}\right) - \frac{2}{3}\mu_{\text{eff}}\frac{\partial u_k}{\partial x_k}\delta_{ij} \tag{14}$$

$$-\overline{\rho u_\iota' u_J'} = \mu\left(\frac{\partial u_j}{\partial x_i} + \frac{\partial u_i}{\partial x_j}\right) - \frac{2}{3}\left(\rho k + \mu_t\frac{\partial u_k}{\partial x_k}\right)\delta_{ij} \tag{15}$$

Shear Stress Transport (SST) k-ω turbulence model [15] is used for turbulence closure, which has been shown to predict the oscillating velocity profiles near the wall and the core, better than the other turbulence models when compared with the experimental data [18,19]. The choice of turbulence model against the laminar model for this study is discussed in Section 4. Pressure-based solver, Pressure Implicit Splitting Operators (PISO) algorithm, and second-order discretisation are used for the transport and turbulent equations in all simulation cases. The convergence criteria of 10^{-5} and 10^{-8} are used for the transport and energy equations, respectively. Default values are retained for all other constants in the SST k-ω turbulence model [3,34].

3.4. Boundary and initial conditions

The pressure amplitudes and phases measured by P2 and P7 (cf. Fig. 4) are assigned to the domain inlet and outlet as the acoustic boundary conditions which are described by:

$$P_{in} = p_{1,in} \cos(\omega t + \phi_{in}) \tag{16}$$

$$P_{out} = p_{1,out} \cos(\omega t + \phi_{out}) \tag{17}$$

where $p_{1,in}$, $p_{1,out}$, ϕ_{in} and ϕ_{out} are the measured pressure amplitudes and their corresponding phases. The turbulence conditions at the domain inlet and outlet are specified in terms of the intensity and length scale as:

$$I = 0.16\big(Re_{1(in,out)}\big)^{-1/8}, \ell = 0.07D \tag{18}$$

The acoustic Reynolds number is defined as $Re_{1(in,out)} = \rho_0 u_{1(in,out)} D / \mu_0$ for the domain inlet and outlet locations. The acoustic velocities in the $Re_{1(in,out)}$ is calculated as:

$$u_{1,in}(x) = \frac{p_0}{\rho_m a} \sin(k' x_{in}) \tag{19}$$

$$u_{1,out}(x) = \frac{p_0}{\rho_m a} \sin(k' x_{out}) \tag{20}$$

The value of density and dynamic viscosity at the reference temperature (300 K) are used in Eqs. (19) and (20). p_0 is the measured pressure amplitude at the antinode. The thermal boundary conditions on the CHX1, HHX and CHX2 walls are specified as constant wall temperatures, which are measured from the experiments. At the inlet and outlet of the domain, additional temperature conditions $\partial T / \partial x|_{x_{in},x_{out}} = 0$ are specified such that the temperature of the cells next to the boundaries is equal to that of the reversing flow. The resonator wall is modelled as adiabatic and non-slip boundary conditions are applied to all walls in the model.

4. Results and discussion

The results in this section are arranged into eight sub-sections. Section 4.1 discusses the pressure amplitude obtained at different axial locations. Sections 4.2, 4.3 and 4.4 focus on the temperature, heat flux and Nusselt number, respectively, at various DR. Section 4.5 discusses the dependency of Nu on different Th. Section 4.6 compares the numerical Nu with the models from the literature, while Section 4.7 discusses further simulation results to extend the understanding of the heat transfer and pressure drop in oscillatory flow. The simulation results are obtained within a flow cycle as shown in Fig. 6. A flow cycle is discretized into 20 equal phases (ϕ) of which ϕ1−ϕ10 constitute the suction stage, and ϕ11−ϕ20 represent the ejection stage.

To build confidence in the numerical results, a systematic mesh convergence study was carried out using T-HEX (ogive). A very fine mesh size (< 0.12 mm) was required in the gas channels for accurate resolution of the flow phenomena, which led to a maximum improvement of less than 1% between the 'coarse' and the 'fine' mesh size at the refinement ratio of 1.8. The mesh resolution is sufficient to achieve mesh-independent results [12,27]. Every simulation case involved about 4.5 million mesh cells (with more than 98% located in the region occupied by the heat exchangers) and simulation run of more than 90,000 time steps, representing a real time of 2.8 s.

4.1. Pressure amplitude profile

Fig. 7 shows the comparison of pressure amplitude distribution in the region between 4.2m < x < 4.4m (marked with a dashed line in Fig. 4) for measured (symbols) and numerical (solid lines) results. In all the plots, it can be observed that the pressure profile is distorted around the heat exchangers at x=4.244, 4.276, 4.308 and 4.340 m, which is due to the flow resistance caused by the sudden change in the cross-section of the flow channel. It should be noted that the pressure profiles are asymmetrical, which is because the centre of HHX (x=4.29 m) did not coincide with the centre of the test rig (x=4.45) where the velocity is nonzero (velocity antinode or pressure node). Therefore, the pressure profile at 0 < x < 4.29m is on the rising side of the standing wave, which makes it higher than the profile at 4.29 > x > 4.45 m. In a standing wave thermoacoustic system, the internal elements (heat exchangers and stack) must be placed at a location where the oscillating pressure and velocity are non-zero.

17

The choice of a suitable viscous model for every simulation case at a specific DR is important to achieve accurate numerical predictions. For this reason, simulation cases for laminar and turbulence models were first performed. Fig. 7a shows the pressure amplitudes from both simulation and experiments for T–HEX (Flat) at T_h = 70 °C, which reveal that the turbulence model gave better agreement with the experimental data than the laminar model, noticeably in the vicinity of the heat exchangers. The acoustic pressure from the laminar model deviates increasingly from the experiment results as the DR increases, which suggests that the turbulence model well resolves the complex flow behaviour around the heat exchangers. Mohd Saat [18,19] obtains a similar result for a parallel-plate structure, where the turbulence models yielded results that agreed well with the experimental data than the laminar model counterpart. Also, Merlki and Thomann [16] suggested that the flow regime in oscillatory flow should be considered laminar if the critical Stokes Reynolds number ($Re_c = 2u_{m,h}/(v\omega)^{1/2}$, where v is the kinematic viscosity) is less than 400. Table 3 shows the Rec in the experiments for T-HEX (flat) at T_h = 70 °C. At DR $\leqslant$ 0.64%, the Rec is lower than the suggested transition regime, while at DR > 0.64% the Re_c is greater. In this paper, a turbulence model is used in all the simulation cases based on the comparison between the turbulence and laminar models against experimental data (cf. Fig. 7a), which favoured the use of the former.

Fig. 7b and c show the experimental and numerical results for two different thermal conditions on T-HEX (flat), the adiabatic and the imposed temperature-gradient conditions. In the adiabatic condition, the heat exchanger walls are considered as adiabatic to mimic the experiments where the heat exchangers are tested at room conditions with no imposed temperature difference, mainly to serve as a reference for result comparison. For the imposed temperature gradient condition, the CHX1, CHX2 are maintained at $T_{c1,c2}$ = 10 °C, and HHX is kept at T_h = 70 °C to allow direct comparison with the experimental data. In both plots (Fig. 7b and c), there are good agreements between the numerical and experimental results with averaged discrepancies of less than 5% at the maximum DR. Fig. 7d shows the measured and numerical results for T-HEX (ogive). Like Fig. 7b and c, a good agreement can be seen in the plot, with an average discrepancy of less than 10% at the highest DR. The agreement between the measurement and simulation results is needed to yield confidence in the simulation results.

The influence of the edge shape on the pressure amplitude profile can be examined by comparing the simulation results in Fig. 7c and d. It can be observed that the magnitude of distortion of pressure profile near the heat exchangers is different considerably for the two geometries. In both cases, the distortion is highest at x=4.276m and x=4.308 m, which corresponds to the gaps between CHX1/HHX and HHX/CHX2, respectively. The ogive edge minimised the pressure drop by 70 and 185 Pa, respectively, at both locations for DR=1.29%. It can be observed from the plot that the minimisation of pressure drop by the aerodynamic shape gets significant as the DR increases, which indicates that the nonlinear effect such as vortex formation and shedding, is increasingly minimised, as will be discussed in Section 4.7. This is quite interesting from the viewpoint of a practical thermoacoustic system which often operates at high amplitudes (DR > 5%) [4,36].

4.2. Temperature profile

In Fig. 8, the difference between the experimental and simulation gas temperatures are presented for various locations near the heat exchangers (x=4.244, 4.276, 4.308m and 4.340 m). There exists a good agreement between both results with maximum discrepancies of 6.7% and 5.3% for T-HEX (flat) and T-HEX (ogive), respectively. The difference occurs at the low DR (< 0.31%), where the gas displacement and the imposed temperature gradient are low. It should be noted that the difference between T_h and $T_{c1,c2}$ (i.e. $T_h - T_{c1,c2}$) is used as a reference in the evaluation of the deviation. In both plots, the numerical temperature profile shows a similar trend to the experiments, with rapid decrease/ increase in the hot/cold gas temperature at DR ≤ 0.64%, which indicates rapid movement of the hot gas from the hot region to the cold region. In both cases, the measured CHX1 and CHX2 temperatures are higher in magnitude than the numerical values, while the measured HHX temperatures are lower than the numerical at DR < 0.65%. Above this point, both results are almost the same for CHX1 and CHX2 as well as for the HHX for the two configurations.

The influence of the heat exchangers edge shape on the gas temperatures can be discussed from Fig. 8a and b. In the plots, the predicted gas temperatures for T-HEX (ogive) are higher for HHX and lower for

CHX1 and CHX2 at the investigated DR, in comparison with the T-HEX (flat), the maximum difference of about 3 °C (i.e. 4% at a reference temperature difference $T_h - T_{c1,c2}$).

4.3. Heat flux (q)

In the simulation, the heat flux is obtained as a function of both space and cycle [3,29,41], which can be defined as:

$$q_{h,c1,c2} = \frac{1}{2\pi A_s} \int_0^{2\pi} \int_{A_s} q(x,\phi)|_{\text{wall}} dA d\phi \tag{21}$$

The local instantaneous heat flux, $q(x, \phi)$, as a function of area and phase are obtained directly from simulation result and then averaged over a flow cycle. Fig. 9 shows the comparison between the experimental and numerical heat fluxes for the two heat exchanger types. The positive heat fluxes reflect the heat being transferred from HHX wall to the oscillating gas while the opposite is the heat transfer from the gas to the CHXs wall. There are good agreements between the experimental and the numerical heat fluxes which is, however, better at DR < 0.64% than at higher DR's. The trend from both results is similar, with a gradual increase in the heat fluxes. The increase or decrease of DR reflects the increase or decrease in the gas displacement amplitude (cf. Eq. (5)). A similar effect of DR on heat transfer was observed by Piccolo [25], where a variation of heat flux (heat load per unit area) as a function DR is reported through a numerical study.

The comparison between the numerical results in Fig. 9a and b shows that the T-HEX (ogive) yielded lower heat fluxes noticeably at DR < 0.8%. However, as the DR increases, the difference between the heat fluxes for the two edge shapes becomes less pronounced, which are 15.67 and 15.15 kW/m^2 at DR=1.29. According to the heat balance from the symmetric arrangement of the heat exchangers, $\dot{Q}_h = \dot{Q}_{c1} + \dot{Q}_{c2}$, the magnitude of heat absorbed by the CHXs is higher than the heat supplied to the oscillating gas by the HHX with a maximum difference of 3.3% and 2.5% for T-HEX (flat) and T-HEX (ogive), respectively. This deviation in the heat input and the heat removed may be attributed to the

nonlinear effects such as streaming, which can advect heat away from the heat exchangers. The magnitude of the heat imbalance is lower for the T-HEX (ogive) and suggests this fact. The result here is very interest considering that the heat transfer performance of both edge shapes become increasingly similar as the DR increases. Meanwhile, the ogive shape further shows an increasing performance regarding the pressure drop as will be seen later.

4.4. Nusselt number (Nu)

Like the heat flux in Section 4.3, the Nu in Eq. (3) is presented as a function of flow cycle and the heat exchanger area in contact with the oscillating gas as:

$$Nu_{h,c1,c2} = \frac{1}{2\pi A_s} \int_0^{2\pi} \int_{A_s} Nu(x,\phi) dA d\phi \, ; \;\; Nu(x,\phi) = \frac{h_c(x,\phi)d_h}{k} \tag{22}$$

where $Nu(x, \phi)$ and h_c are the local instantaneous Nu and the heat transfer coefficient defined as:

$$h_c(x,\phi) = \frac{q(x,\varphi)}{\Delta T(x,\varphi)} \tag{23}$$

The thermal potential for the heat transfer coefficient is defined in terms of space and time as $\Delta T(x,\phi) = T_s(x) - T_i(\phi)$. $T_i(\phi)$ is the mean of gas temperature defined as: $T_i(\phi) = \left(T_{g,in}(\phi) + T_{g,out}(\phi)\right)/2$, where $T_{g,in}(\phi)$ and $T_{g,out}(\phi)$ are the inlet and outlet instantaneous gas temperatures of the heat exchangers.

Fig. 10 shows the Nu comparison for T-HEX (flat) and T-HEX (ogive). Both measured (symbols) and numerical (solid line) results have a similar increasing trend with an increase in the DR. At low DR < 0.6%, the numerical model slightly under predicts the heat transfer, whereas, it overpredicts the performance at higher amplitudes (DR > 0.6%). The result is consistent with the findings in the literature [25]. However, the magnitude of deviation of both low and high amplitude in the current study is considerably lower. It should be noted that since the heat exchangers are identical, it is quite interesting

21

to have similar trends in the Nu for CHX1, HHX and CHX2 in both results. The average discrepancies between the experimental and numerical results are 18% and 23% for T-HEX (flat) and T-HEX (ogive), respectively. The deviation in the results may be attributed to few factors which may include the method of heat transfer evaluation in the simulation, the model capability to resolve the complex flow phenomena, and thermoacoustic effect in the physical experiments.

4.5. Effect of temperature on the Nu

Fig. 11 shows the change in Nu against DR due to temperature. The temperature on HHX (Th) is varied from 30 to 70 °C at 20 °C step in both experiment and simulation. T-HEX (flat) is used for the investigation. In both cases, a similar trend can be observed with a uniform increase in Nu over the DR as the T_h increases, which is more pronounced in the experimental result. The observed increase in the Nu can be attributed to the change in the temperature dependent properties of the working fluid such as the viscosity, density and the heat capacity. Also, since the heat exchangers interact thermoacoustically with the oscillating flow, acoustic energy is generated/consumed due to thermoacoustic/thermoviscous effects with thermal energy as well.

4.6. Comparison of Nu against previous studies

Fig. 12 shows the comparison between the current numerical heat transfer result and the existing models in the literature. For the comparison, the Nu for T-HEX (flat) at T_h=70 °C are compared against the acoustic Reynolds number. The existing correlations that are considered include the Time-Average Steady-Flow Equivalent (TASFE) model [28] and the experimental correlation proposed by Nsofor et al. [23]. The Nu and acoustic Reynolds number (cf. Eqs. (3) and (7)) from the selected studies are calculated based on the same length scale (d_h). Piccolo and Pistone [26] presented Nu correlation for the TASFE model as:

$$Nu = \frac{\overline{\omega}}{\pi} \int_0^{2\pi} \left\{ 3.66 + \frac{0.0668(d_h/l)PrRe_1 \sin \omega t}{1 + 0.04[(d_h/l)PrRe_1 \sin \omega t]^{2/3}} \right\} dt \tag{24}$$

Nsofor et al. [23] correlated their experimental data in terms of Nu defined based on the RMSRe ($Re_{rms} = Re_1/\sqrt{2}$), for heat transfer performance of a finned-tube type heat exchanger of a thermoacoustic refrigeration system, which can be written as:

$$Nu = 0.61\left(Re_1/\sqrt{2}\right)^{0.31} Pr^{0.11} \qquad (25)$$

The TASFE approximation is based on a steady flow and may reflect the increase in Nu with an increase in the acoustic Reynolds number. The results in Fig. 12 reveal that the current CFD model and TASFE approximations predicted higher Nu by 24.9% and 35.0%, respectively, in comparison with the experimental correlation of Nsofor et al. [23]. The TASFE model has been reported with a similar deviation by Piccolo and Pistone [26]. However, the observed discrepancy of the current numerical model may be attributed to the difference in the type of geometries. The CFD model is based on the Tube Heat exchanger type, while Finned tube type was utilised in the experiment of Nsofor et al. [23]. Also, the range of operating conditions and differences in the methods of evaluation could contribute to the difference.

4.7. Numerical predictions

The numerical investigations to extend the knowledge from the experimental results are discussed in this section. The maximum velocity amplitude, flow structure, Nusselt number, and pressure drop due to minor losses are discussed. The results are discussed for the suction stage of the flow cycle for brevity.

The maximum velocity amplitudes for T-HEX (flat) and T-HEX (ogive) are shown in Fig. 13. The comparison is made at x=4.32m to demonstrate the influence of the edge shape on flow conditions near the velocity antinode (x=0.2472 λ). In principle, other locations near the heat exchangers can be chosen to demonstrate the geometric effect on velocity amplitude. Fig. 13a shows the velocity amplitudes at T_h = 70 °C, which increase monotonically for both heat exchanger configurations, but with higher magnitudes for T-HEX (flat) at all DR's. The higher velocity amplitude in the case of T-HEX (flat) can

23

be attributed to the fact that the flow transition over the 90° edge will be more sudden at the change in cross-section, which causes an increase in the gas velocity due to a smaller flow area (in comparison to ogive edge), according to the law of mass conservation. On the other hand, the transition of flow over a streamlined body is more gradual and lead to a smaller increase in the gas velocity. The displacement amplitudes that correspond to the velocity amplitudes in Fig. 13 are in the range of 14.17–93.50mm and 8.37–62.63mm for T-HEX (flat) and T-HEX (ogive), respectively. The effective length of the heat exchanger is 28mm which corresponds to the DR=0.31% and 0.48% for T-HEX (flat) and T-HEX (ogive), respectively. Fig. 13b shows the effect of T_h on the velocity amplitudes at DR=1.29 for the two investigated configurations. The increase in the gas temperature causes an increase in the gas velocity amplitude, which appears to be linear for both edge shapes over in the investigated temperature range (T_h = 30–150 °C). The increase in the gas velocity can be explained from the viewpoint that the fluid viscosity gets lower as the temperature increases and the gas experiences lesser viscous drag which causes it to move faster for a fixed acoustic excitation.

The vorticity contours can be used to further illustrate the effect of edge shape on flow structure around the heat exchangers. Fig. 14 shows the vorticity plots in the x–y plane (cf. Fig. 4) to show the vortex structure within the gap between two adjacent heat exchangers and the edge of the CHX2 open to the resonator. The vorticity is calculated as $\omega = \partial v/\partial x - \partial u/\partial y$, where u and v are the velocity components in the x–y plane. Vorticity plots at $\phi 2$, $\phi 5$ and $\phi 8$ in the suction stage of flow cycle at DR=0.64% are used for the comparison. At each phase, a pair of vortex structures of equal size but opposite strength is formed in the flow channel and remain attached. They are symmetrical about the centreline of the channel in the x-y plane. At the end of the channel (right side of CHX2), it can be observed that the formation of vortex structure is delayed and the strength is minimised for T-HEX (ogive) at all the three phases when compared with the T-HEX (flat). The vortex structures appearing in the 'wake' of the heat exchanger can create a disturbance when it is pushed back into the gas channel by the reversing flow during the ejection stage. The higher the vortex strength, the greater the disturbance and the dissipation that will be created in the flow channel. The presence of profile edge (ogive) minimised the vortex formation and shedding as well as flow velocity (cf. Fig. 13) at the

24

entrance and exit of the HEX flow channel, which led to a reduction in the pressure drop that will be discussed in the later section. There is also a smoother transition of flow structure at the gap between two adjacent heat exchangers with ogive shape. Vortices have been shown to induce streaming which in turn had an adverse impact on the efficiency of thermoacoustic systems [10,24].

Fig. 15 shows the dependence of Nu on thermal conditions at various DR. The results indicates a rapid increase in the Nu as the T_h increases to about 100 °C after which it becomes gradual. The variation, however, does not show a significant dependence on the DR at $T_h < 70$ °C, which indicates that the heat transfer in this threshold is mainly due to the thermal excitation rather than the acoustic excitation. At $T_h > 70$ °C, the contribution of the acoustic excitation to the heat transfer increases, especially at the cold heat exchangers and more significantly for the T-HEX (ogive). The highest heat transfer is achieved at DR = 0.64% (T_h = 100 °C) with the T-HEX (flat) having a 2.5% higher performance. However, on the HHX, the performance of the two heat exchangers are very similar, especially at low acoustic excitation range. The results further support the fact that the heat exchangers interact thermoacoustically with the flow and both acoustic and thermal energies contribute to the heat transfer. It is interesting that the T-HEX (ogive) shows a heat transfer performance comparable to that of T-HEX (flat).

Fig. 16 shows the pressure drop (Δp) due to minor losses (cf. Eq. (9)) across the heat exchangers. The influence of edge shapes and DR on Δp at various thermal conditions (30–150 °C) are considered, including the adiabatic condition which is added in the plot for reference. The pressure amplitudes are the static oscillating pressure in the fluid domain. The results are presented for the suction stage in the flow cycle (cf. Fig. 6) for brevity. Fig. 16a–c represent the pressure drop across the THEX (flat) set while Fig. 16d – f denote that of T-HEX (ogive). From the plots, the pressure drop shows a dependency on the DR and edge shape for all thermal conditions. As the drive ratio is increasing, the pressure drop increases significantly due to the increasing flow complexities such as the minor losses created by the sudden change in cross section of the flow channels. This can be observed for the two edge shapes with a higher magnitude for the T-HEX (flat). Clearly, from the plots (Fig. 16), the T-HEX (ogive) has pressure drop magnitude that is 43% lower for CHX2 at DR=1.29% and T_h=70 °C. The effect of T_h can

25

also be seen in the plots, which is more pronounced for the HHX at DR > 0.31% due to the increase in temperature, but less for the CHX's because of the constant temperature. Due to the symmetry of the heat exchanger arrangement, the Δp across HHX does not differ considerably for the two edge shapes, though the ogive edge shape still has lower magnitude. The increase in temperature increases the pressure drop due to change in the fluid viscosity which in turn causes an increase in the gas velocity, hence increased non-linearity in the flow (cf. Fig. 14).

It should be noted that the pressure drop is dependent on the sampling location, as it exists in a standing wave because the ratio of kinetic energy (velocity amplitude) to the potential energy (pressure amplitude) is a function of the position in the setup. However, since the same locations are used for the comparison in the current study, the results thus reflect the role of ogive edge shape in the minimising the pressure drop across the heat exchangers, especially, at high acoustic amplitudes.

5. Conclusions

This paper investigates the characterisation of Tube-Heat Exchangers (T-HEX) in oscillatory flow, using experimental and numerical methods. A 3D computational model has been developed and validated based on the purpose-built experimental setup. Good agreement between the experimental and numerical results are achieved. The heat transfer and pressure drop performance of T-HEX show dependency on DR, HHX inlet temperature (T_h) and edge shape of the gas channel, as observed in both experimental and numerical results. It is observed that the presence of profile edge shape causes a slight adverse reduction in the heat transfer performance at low DR. However, the effect diminishes gradually as the DR increases, and a comparable performance is observed for the two edge shapes at high amplitudes. The presence of ogive edge minimised the vortex formation and shedding as well as flow velocity at the entrance and exit of the HEX gas channels, which led to a significant reduction in the pressure drop, especially, at high amplitudes. The result here is interesting from the viewpoint of the practical thermoacoustic engines and coolers, which often operates at high amplitudes (DR > 5%). It demonstrates the possibility of using the heat exchanger edge shapes to minimise the pressure drop (due to minor losses) without affecting the heat transfer and shows that the use of Tube-Heat-Exchanger with

26

profiled gas channels (T-HEX (ogive)) will be beneficial to the overall performance of thermoacoustic systems.

Acknowledgement

References

[1] P.C.H. Aben, P.R. Bloemen, J.C.H. Zeegers, 2-D PIV measurements of oscillatory flow around parallel plates, Exp. Fluids 46 (4) (2009) 631–641.

[2] T.M. Adams, Guide for Estimation of Measurement Uncertainty in Testing (G104–A2LA): Maryland, American Association of Laboratory Accreditation, USA, 2002.

[3] ANSYS Fluent 15.0, User Manual, ANSYS Inc, 2015.

[4] S. Backhaus, G.W. Swift, A thermoacoustic-Stirling heat engine: detailed study, J. Acoust. Soc. Am. 107 (6) (2000) 3148–3166.

[5] J.R. Brewster, R. Raspet, H.E. Bass, Temperature discontinuities between elements of thermoacoustic devices, J. Acoust. Soc. Am. 102 (6) (1997) 3355–3360.

[6] R.H. Dieck, W.G. Steele, G. Osolsobe, Test Uncertainty. ASME PTC 19.1-2005, The American Society of Mechanical Engineers, New York, 2005.

[7] A. Al-Damook, N. Kapur, J.L. Summers, H.M. Thompson, An experimental and computational investigation of thermal air flows through perforated pin heat sinks, Appl. Therm. Eng. 89 (2015) 365–376.

[8] D.L. Gardner, G.W. Swift, A cascade thermoacoustic engine, J. the Acoust. Soc. Am. 114 (4) (2003) 1905.

[9] S.L. Garrett, D.K. Perkins, A. Gopinath, Thermoacoustic refrigerator heat exchanger-design, analysis and fabrication, in: Proc. of the Tenth International Heat Transfer Conference, Brighton, UK, 1994.

[10] C. Gu, Y. Zhou, J. Wang, W. Ji, Q. Zhou, CFD analysis of nonlinear processes in pulse tube refrigerators: streaming induced by vortices, Int. J. Heat Mass Transf. 55 (2012) 7410–7418.

[11] O.M. Ilori, X. Mao, A.J. Jaworski, Design of thermoacoustic rig for the analysis of thermal and hydraulic performance of heat exchangers in oscillatory flow, in: Proceedings of the World Congress on Engineering, WCE 2013, July 3–5, 2013, London, UK, vol. III, 2013.

[12] O.M. Ilori, X. Mao, A.J. Jaworski, CFD-Simulation of oscillatory flow around the heat exchangers of thermoacoustic devices, in: Proceedings of the 2014 International Mechanical Engineering Congress & Exposition, IMECE2014, November 14–20, 2014, Montreal, Quebec, Canada.

[13] W. Kamsanam, X. Mao, A.J. Jaworski, Development of experimental techniques for measurement of heat transfer rates in heat exchangers in oscillatory flows, Exp. Therm Fluid Sci. 62 (2015) 202–215.

[14] Kay, London, Compact Heat Exchangers, McGraw-Hill, New York, N.Y., 1964.

[15] F.R. Menter, Two-equation eddy-viscosity turbulence models for engineering applications, AIAA J. 32 (8) (1994) 1598–1605.

[16] P. Merlki, H. Thomann, Transition in oscillating pipe flow, Fluid Mech. 68 (3) (1975) 567–575.

[17] R.J. Moffat, Describing the uncertainties in experimental results, Exp. Therm Fluid Sci. 1 (1) (1988) 3–17.

[18] F.A. Mohd Saat, Numerical Investigations of Fluid Flow and Heat Transfer Processes in the Internal Structures of Thermoacoustic Devices, University of Leicester, 2013 PhD Thesis.

[19] F.A.Z. Mohd Saat, A.J. Jaworski, Numerical predictions of early stage turbulence in oscillatory flow across parallel-plate heat exchangers of a thermoacoustic system, Appl. Sci. 7 (2017) 673.

[20] P.J. Morris, S. Boluriaan, C.M. Shieh, Numerical simulation of minor losses due to a sudden contraction and expansion in high amplitude acoustic resonators, ACTA Acust. Unit. Acust. 90 (2004) 393–409.

[21] G. Mozurkewich, Heat transfer from transverse tubes adjacent to a thermoacoustic stack, J. Acoust. Soc. Am. 110 (2) (2001) 841–847.

[22] J.A. Nijeholt, M.E.H. Tijani, S. Spoelstra, Simulation of a travelling-wave thermoacoustic engine using computational fluid dynamics, J. Acoust. Soc. Am. 118 (4) (2005) 2265–2270.

[23] E.C. Nsofor, S. Celik, X. Wang, Experimental study on the heat transfer at the heat exchanger of the thermoacoustic refrigerating system, Appl. Therm. Eng. 27 (14–15) (2007) 2435–2442.

[24] J.R. Olson, G.W. Swift, Acoustic streaming in pulse tube refrigerators-tapered pulse tubes, Cryogenics 37 (12) (1997).

[25] A. Piccolo, Numerical computation for parallel plate thermoacoustic heat exchangers in standing wave oscillatory flow, Int. J. Heat Mass Transf. 54 (21–22) (2011) 4518–4530.

[26] A. Piccolo, G. Pistone, Estimation of heat transfer coefficients in oscillating flows: the thermoacoustic case, Int. J. Heat Mass Transf. 49 (9–10) (2006) 1631–1642.

[27] P.J. Roache, Perspective: a method for uniform reporting of grid refinement studies, Trans. Am. Soc. Mech. Eng. J. Fluids Eng. 16 (1994) 405–405.

[28] P.D. Richardson, Effects of sound and vibration on heat transfer, Appl. Mech. Rev. 20 (3) (1967) 201–217.

[29] L. Shi, X. Mao, A.J. Jaworski, Application of planar laser-induced fluorescence measurement techniques to study the heat transfer characteristics of parallel-plate heat exchangers in thermoacoustic devices, Meas. Sci. Technol. 21 (11) (2010) 115405.

[30] G.W. Swift, Thermoacoustic engines, J. Acoust. Soc. Am. 84 (4) (1988).

[31] G.W. Swift, Thermoacoustics: A Unifying Perspective for Some Engines and Refrigerators, Los Alamos National Laboratory, 2002 2001(Fifth draft, LA-UR 99-895).

[32] K. Tang, J. Yu, T. Jin, Z.H. Gan, Influence of compression-expansion effect on oscillating-flow heat transfer in a finned heat exchanger, J. Zhejiang Univ. Sci. A (Appl. Phys. Eng.) 14 (6) (2013) 427–434.

[33] K. Tang, J. Yu, T. Jin, Y.P. Wang, W.T. Tang, Z.H. Gan, Heat transfer of laminar oscillating flow in finned heat exchanger of pulse tube refrigerator, Int. J. Heat Mass Transf. 70 (2014) (2014) 811–818.

[34] S.H. Tasmin, R.A. Frazer, Computation of the flow and thermal fields in a thermoacoustic refrigerator, Int. Commun. Heat Mass Transf. 37 (2010) 748–755.

[35] B. Thomas, D. Pittman, Update on the evaluation of different correlations for the flow friction factor and heat transfer of Stirling engine regenerators, in: 35th Intersociety Energy Conversion Engineering Conference and Exhibit, vol. 1, 2000, pp. 76–84.

[36] M.E.H. Tijani, S. Spoelstra, A high performance thermoacoustic engine, J. Appl. Phys. 110 (9) (2011) 093519.

[37] K. Versteeg, W. Malalasekera, An Introduction to Computational Fluid Dynamics. The Finite Volume Method, second ed., Pearson Education Limited, England, 2007 (Chap. 3).

[38] R.S. Wakeland, R.M. Keolian, Measurements of the resistance of parallel-plate heat exchangers to oscillating flow at high amplitudes, J. Acoust. Soc. Am. 115 (5) (2004) 2071.

[39] Worlikar, Knio, Numerical study of oscillatory flow and heat transfer in a loaded thermoacoustic stack, Num. Heat Transf. Part A: Appl. Int. J. Comput. Methodol. 35 (1) (1999) 49–65.

[40] Z. Yu, X. Mao, A.J. Jaworski, Experimental study of heat transfer in oscillatory gas flow inside a parallel-plate channel with imposed axial temperature gradient, Int. J. Heat Mass Transf. 77 (2014) 1023–1032.

[41] T. Zhao, P. Cheng, A numerical solution of laminar forced convection in a heated pipe subjected to a reciprocating flow, Int. J. Heat Mass Transf. 38 (16) (1995) 3011–3022.

[42] F. Zink, J. Vipperman, L. Schaefer, CFD simulation of thermoacoustic cooling, Int. J. Heat Mass Transf. 53 (2010) (2010) 3940–3946.

[43] F. Zink, J. Vipperman, L. Schaefer, CFD simulation of a thermoacoustic engine with coiled resonator, Int. Commun. Heat Mass Transfer 37 (2010) 226–229.

[44] I. Paek, J.E. Braun, L. Mongeau, Characterizing heat transfer coefficients for heat exchangers in standing wave thermoacoustic coolers, J. Acoust. Soc. Am. 118 (4) (2005) 2271–2280.

[45] G. Petculescu, L.A. Wilen, Traveling-wave amplification in a variable standing wave ratio device, Acoust. Res. Lett. Online 3 (2002) 71–76.

[46] Marx David, Bailliet Helene, V. Jean-Christophe, Analysis of acoustic flow at abrupt change in section of waveguide using Particle Image Velocimetry and Proper Orthogonal Decomposition, Acta Acust. Unit. Acust. 94 (2008) 54–65.

[47] D.R. Maidment, Handbook of Hydrology, McGraw-Hill, New York, 1993.

[48] Richardson, M.J., Specific heat capacities. Accessed 05/07/2016<http://www. kayelaby.npl.co.uk/general_physics/2_3/2_3_6.html >.

Table 1 Heat exchangers geometric parameters

Helium gas side	T-HEX
Effective flow length, mm	28
Number circular tubes	89
Tube diameter (d_t), mm	3
Frontal core diameter (f_c), mm	57.4
Porosity (σ), %	24.31
Separation wall thickness, mm	0.5
Effective heat transfer area	
– T-HEX (flat), m^2	0.0273
– T-HEX (ogive), m^2	0.0259

Table 2 Operating parameters and gas properties in the experiment and simulation

Operating parameter	**Values**
Mean pressure (P_m), bar	5
Frequency of oscillation (f), Hz	53.6
Drive ratio, %	$0.15 \leq DR \leq 1.29$
Temperature conditions:	
Hot heat exchanger (HHX)	30–150 °C
Cold heat exchanger (CHX)	10 °C
Helium properties	
Molar mass, kg/mol	0.04
Specific gas constant, J/kg·K	2078.5
Specific heat capacity (c_p), J/kg·K	5193
Speed of sound, m/s	1019.4

(a)

(b)
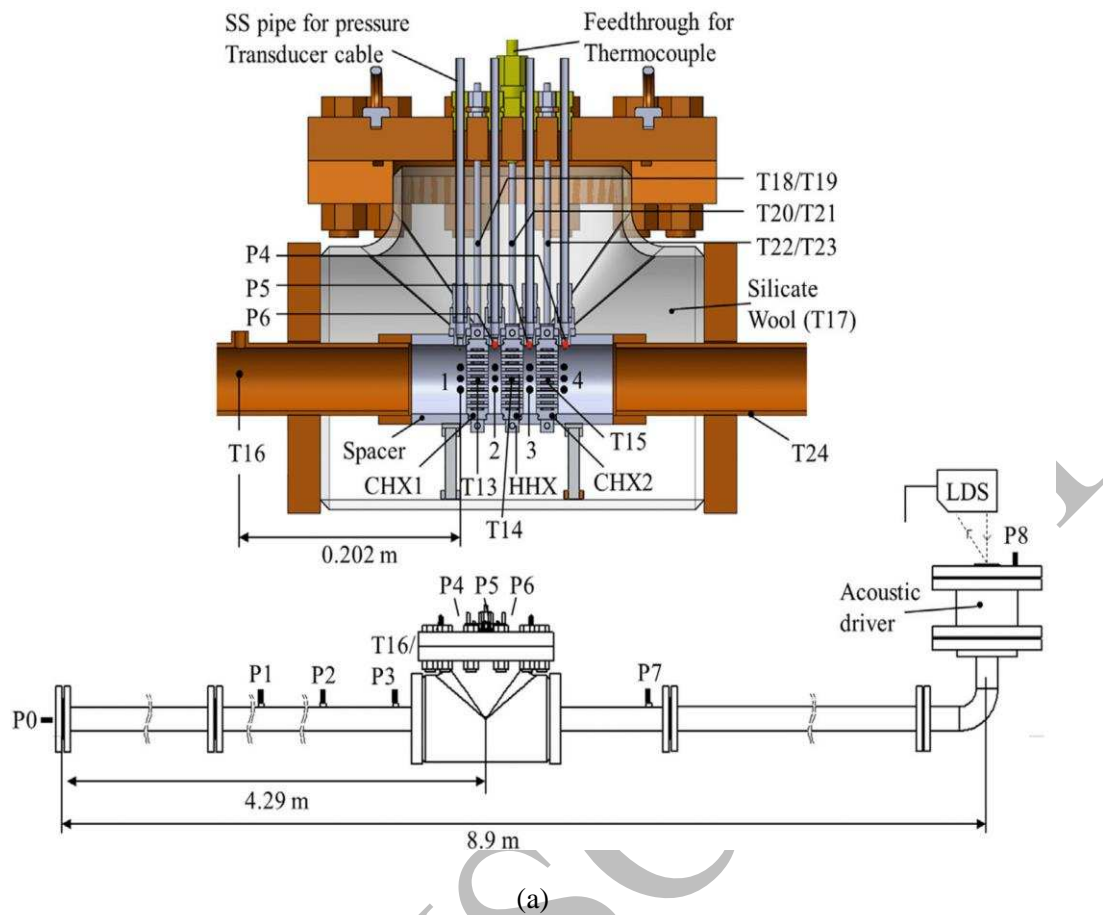
Fig. 1. (a) CAD-image of the test section showing details of CHX1, HHX and CHX2 arrangement (top) and the drawing of experimental set-up (bottom). (b) Photograph of the test section location of the experimental set-up. LDS – Laser Display Sensor. Locations x=4.244, 4.276, 4.308 and 4.340 m, are within the test section and they are used for data sampling during both the experiment and simulation. The oscillating variables at each location are identified with a number of the location as shown in Fig. 1a (top), for example, x=4.244m has temperature T-1 and pressure amplitude P-1.
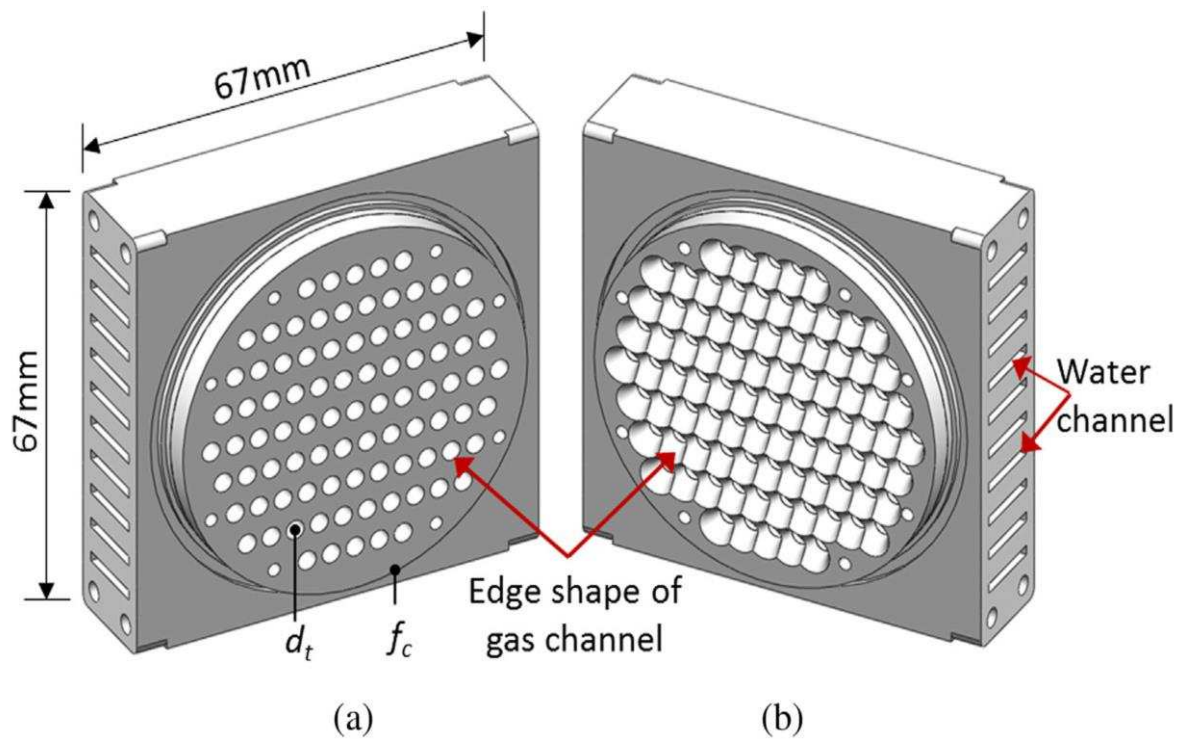
Fig. 2. CAD-image of (a) T-HEX (flat) (b) T-HEX (ogive).
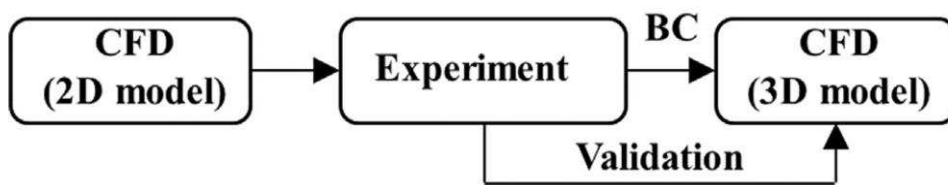
Fig. 3. Approach for integrating the experiments with the Computational Fluid
Dynamics (CFD) model. BC – Boundary Condition.
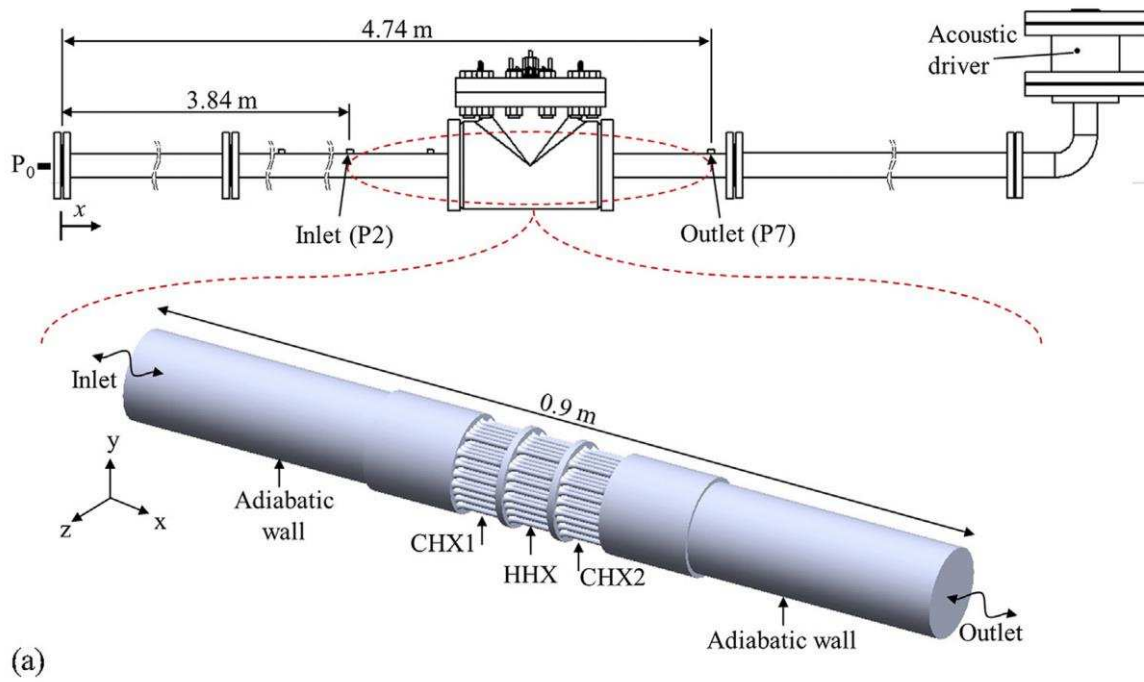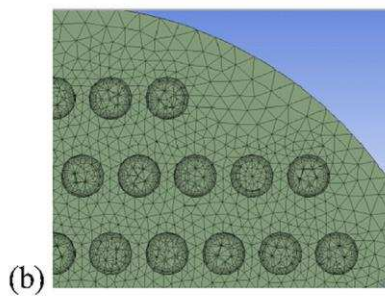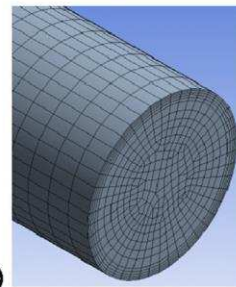
Fig. 4. (a) Sketch of experimental set-up and computational domain (b) cut plane through HEX showing details of the gas channel (c) Inlet/Outlet of the meshed domain.
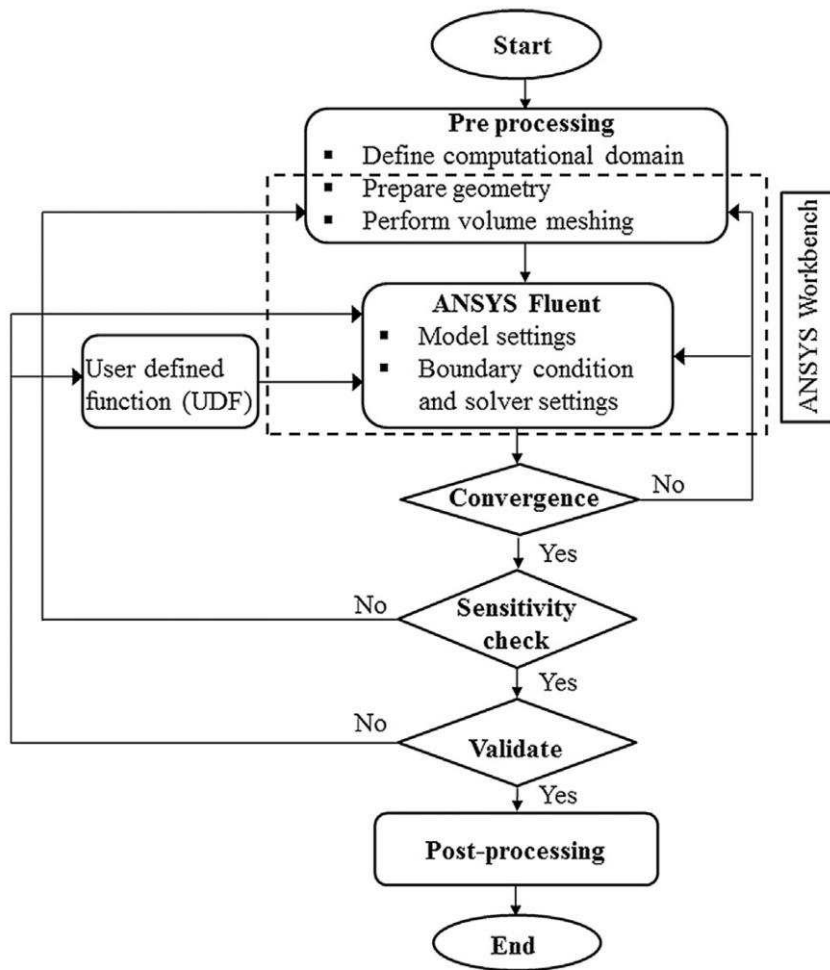
Fig. 5. Flowchart of numerical solution procedure.
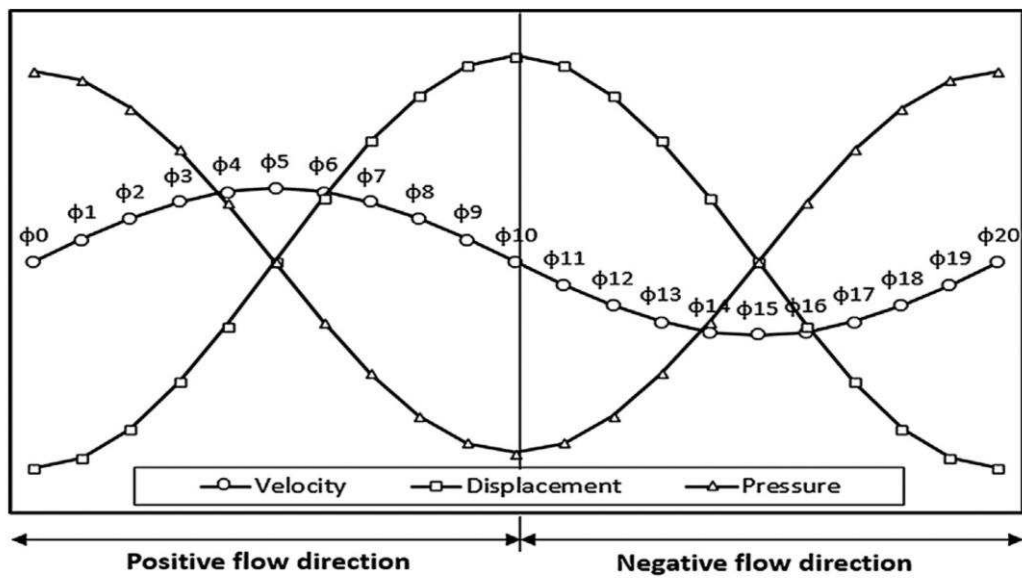
Fig. 6. Relationship between the velocity, gas displacement and pressure amplitudes over the selected 20 phases in a flow cycle.
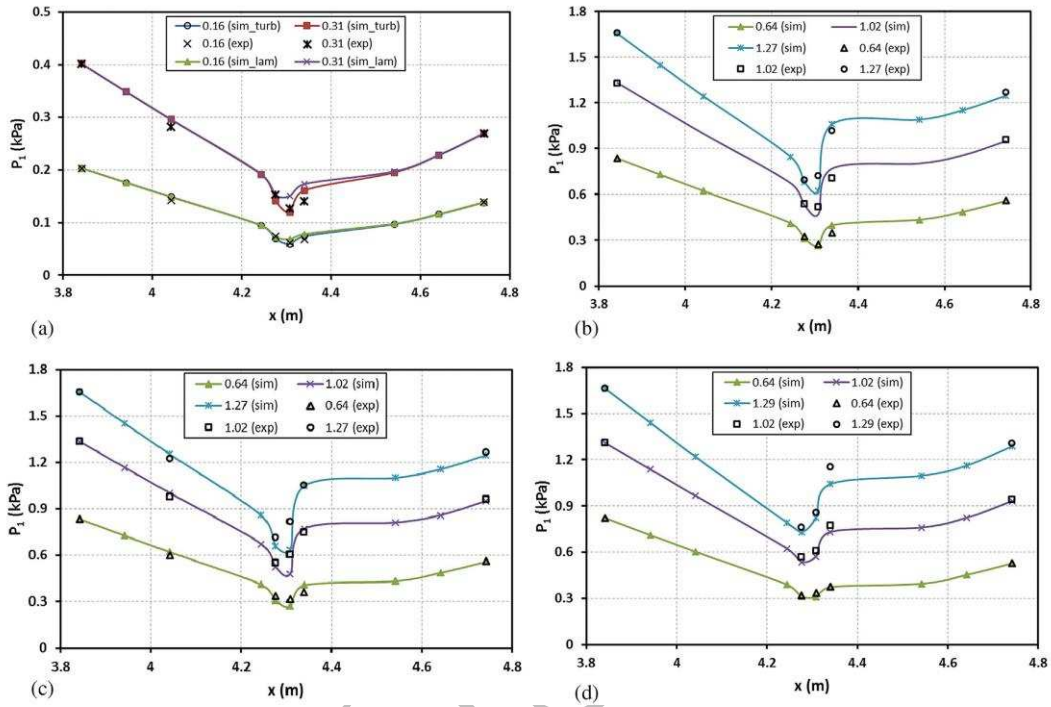
Fig. 7. Comparison experimental (symbol) and numerical (solid line) pressure amplitudes (a) laminar and turbulence models (b) T-HEX (flat) at adiabatic (c) T-HEX (flat) with temperature (d) T-HEX (ogive) with temperature, Th=70 °C, Tc1,c2=10 °C.
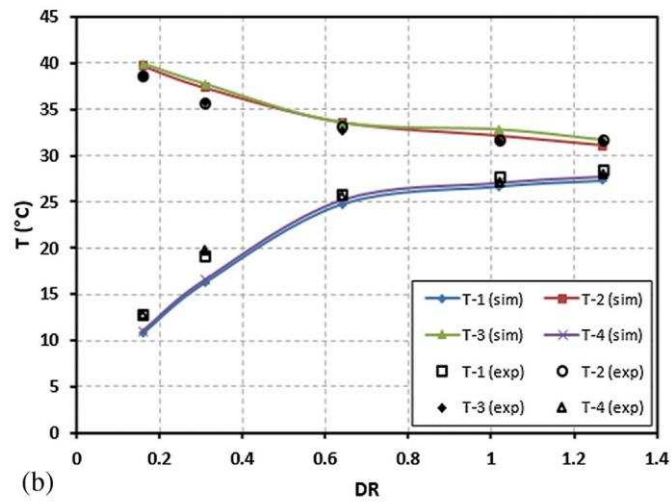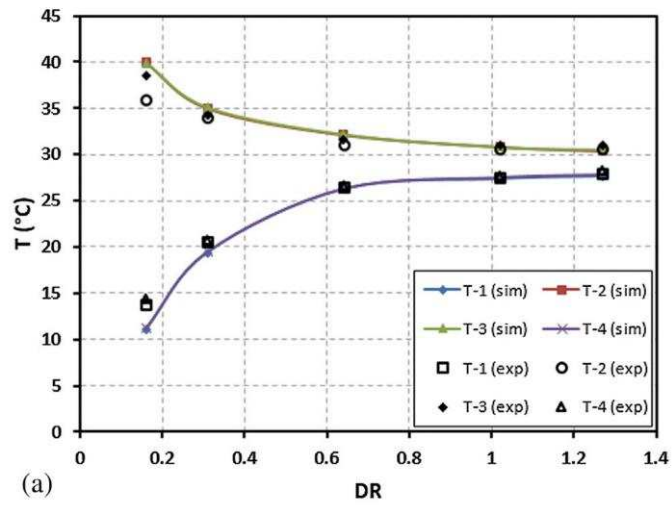
Fig. 8. Comparison between experimental (symbols) and numerical (solid line) temperatures at locations x=4.244, 4.276, 4.308 and 4.340m at Th=70 °C, (a) T-HEX (flat) (b) T-HEX (ogive).

40
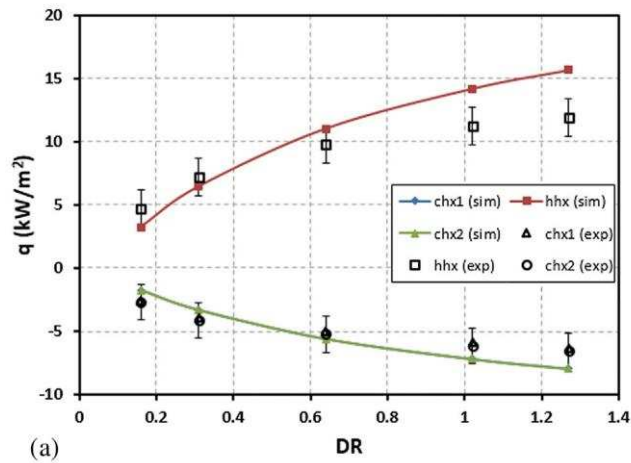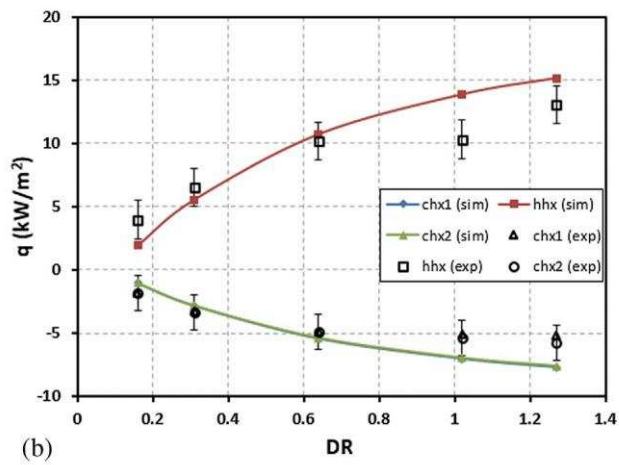
Fig. 9. Comparison heat fluxes from experiment and simulation for (a) T-HEX (flat) (b) T-HEX (ogive).

41
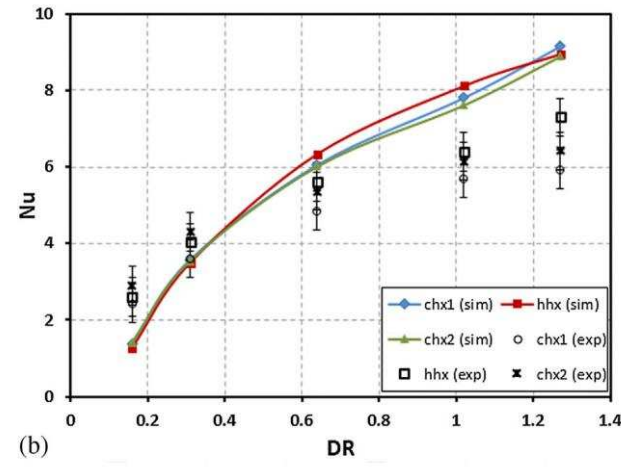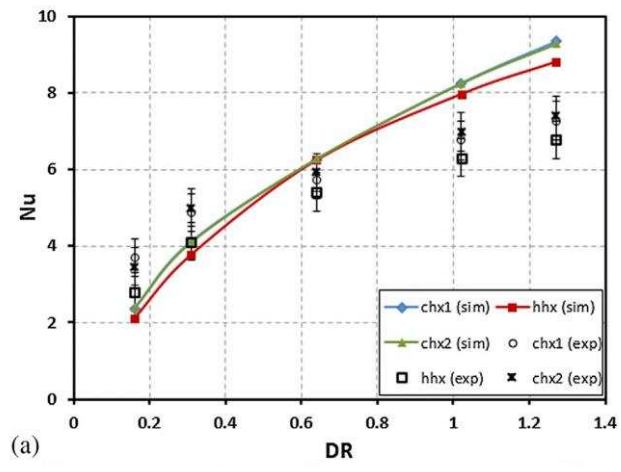
Fig. 10. Nusselt number – experimental vs simulation results for (a) T-HEX (flat edge) (b) T-HEX (ogive).

42
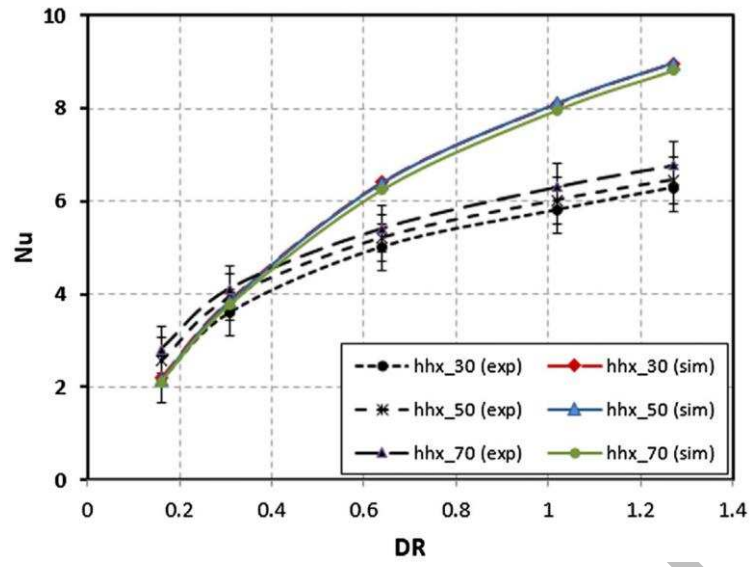
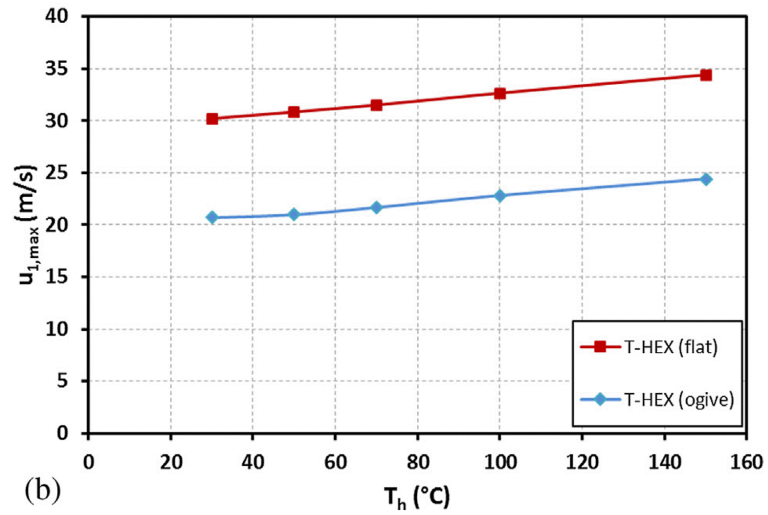Fig. 11. Effect of temperature on Nu at Th=30, 50, and 70 °C for HHX (flat).
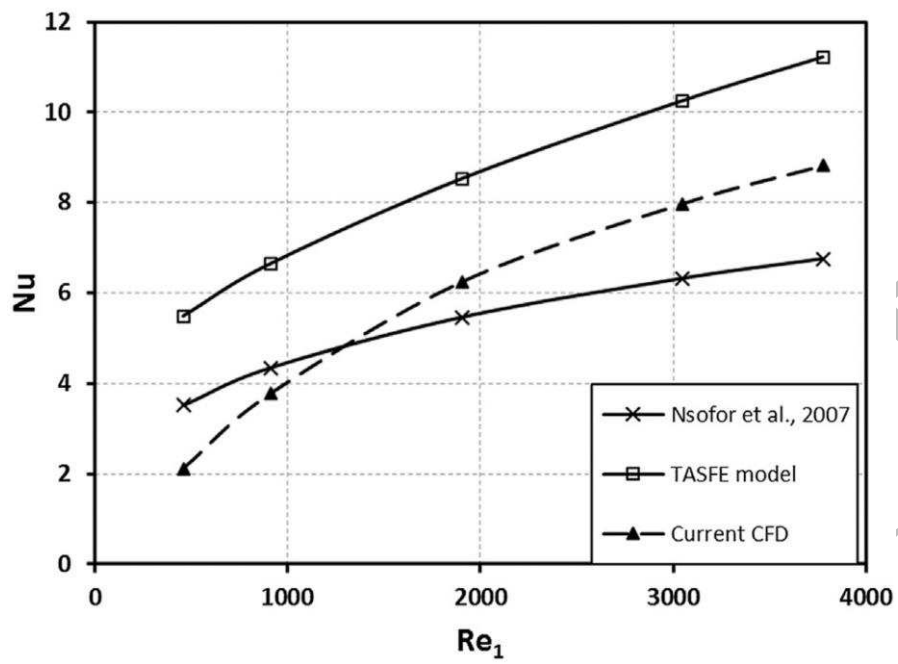
Fig. 12. Comparison between CFD prediction and the models from the literature at Th=70 °C for HHX (flat).
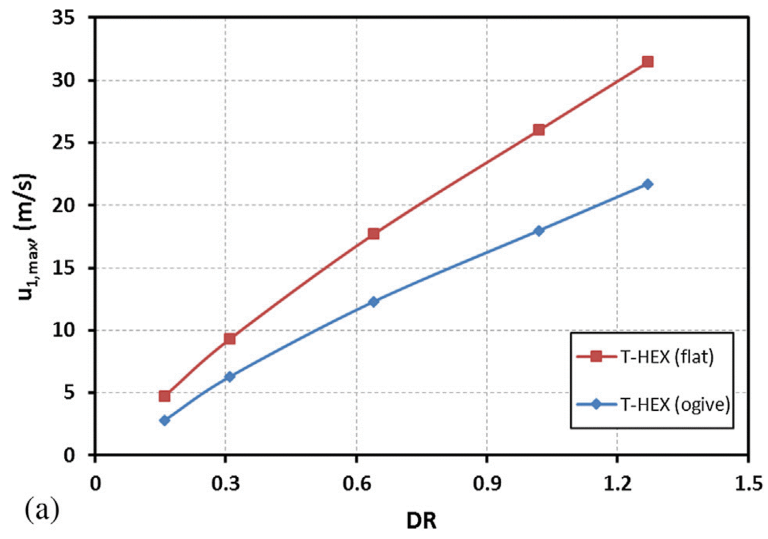
Fig. 13. Velocity amplitudes from the simulation result for T-HEX (flat) and THEX (ogive) (a) effect of DR at Th=70 °C (x=4.32) (b) Effect of temperature at DR=1.29%.
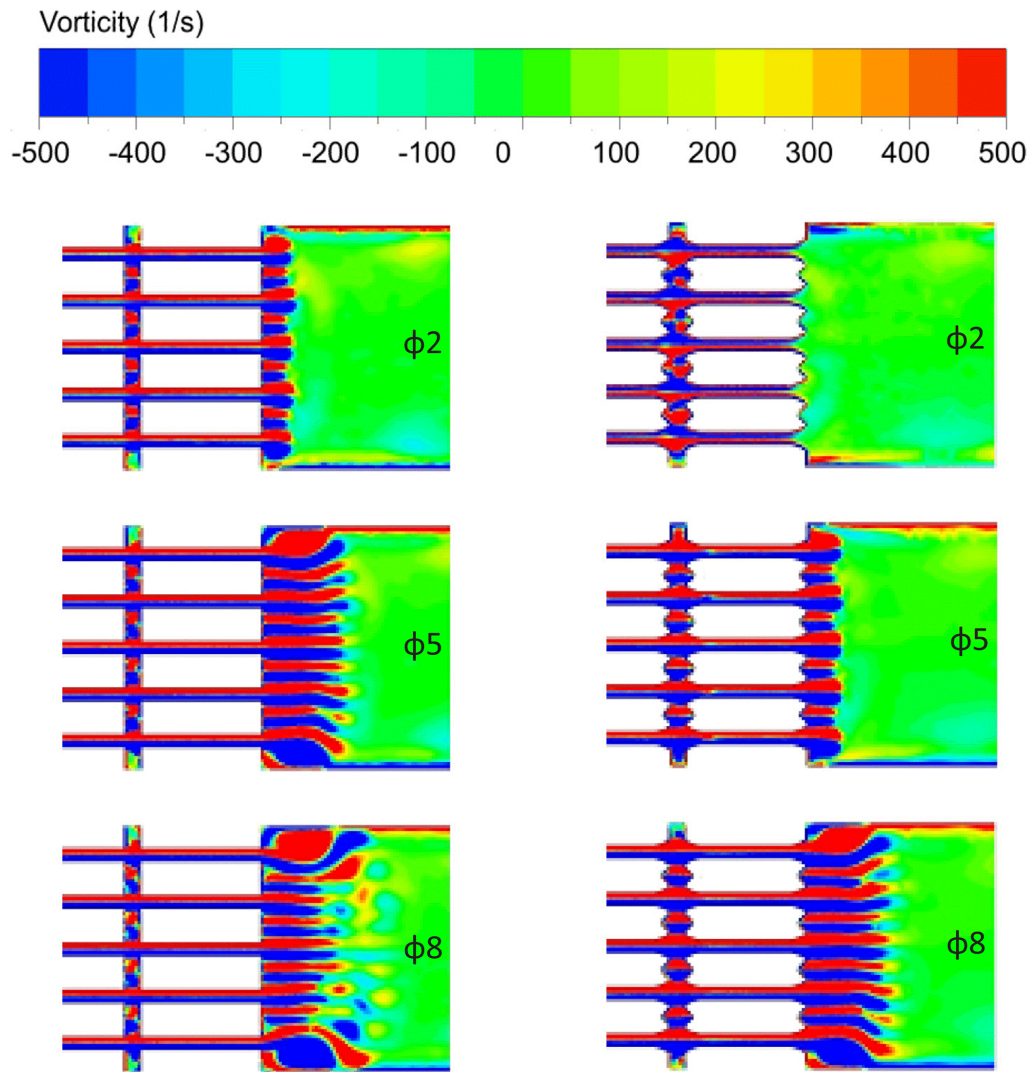
Fig. 14. Vorticity contours – comparison between T-HEX (flat) and T-HEX (ogive) at Th=70 °C, DR=0.64% (a) φ 2 (b) φ 5 (c) φ 8 (x-y plane (cf. Fig. 1c).
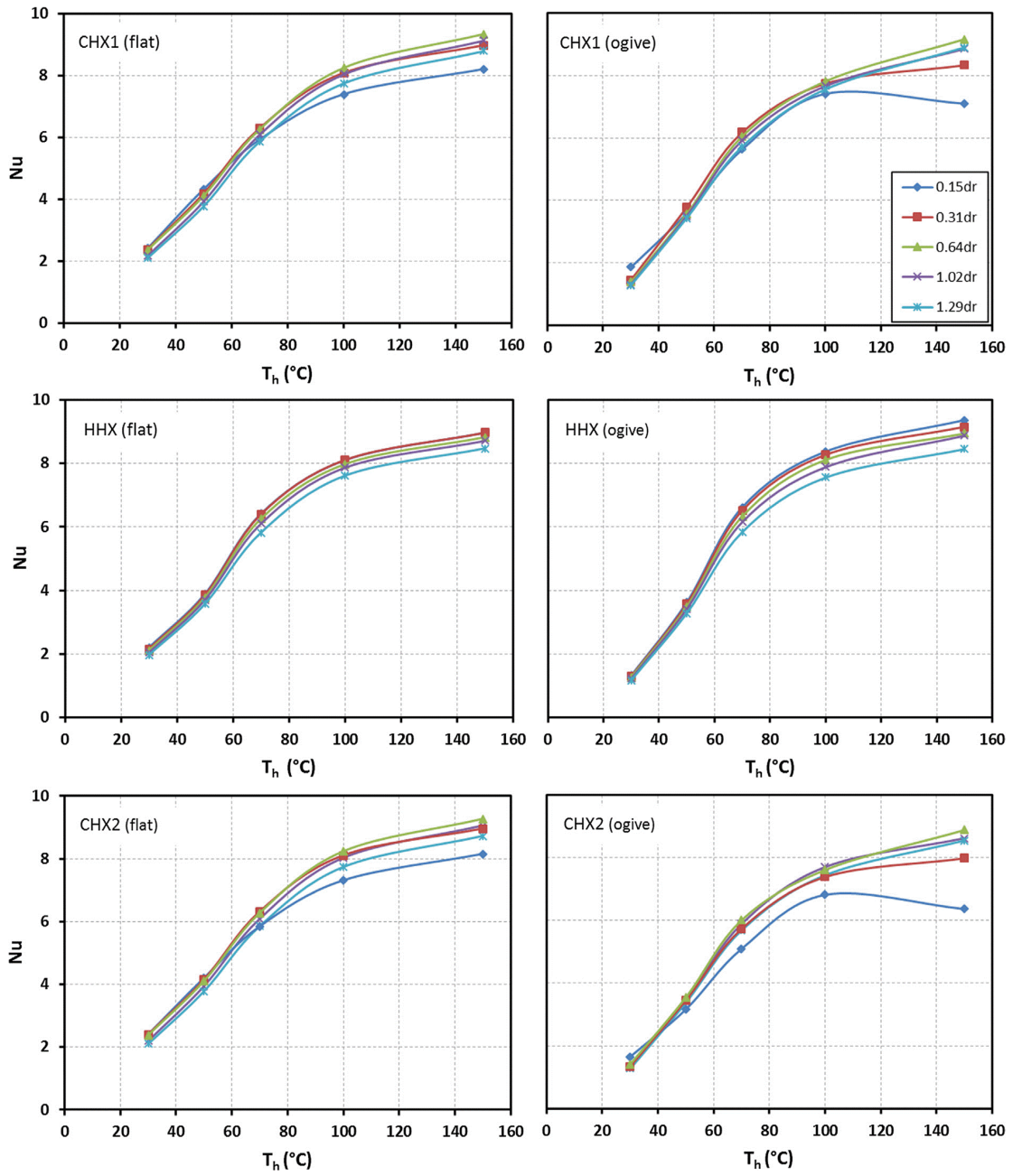
Fig. 15. Effect of temperature on Nu for T-HEX (flat) and T-HEX (ogive) configuration.
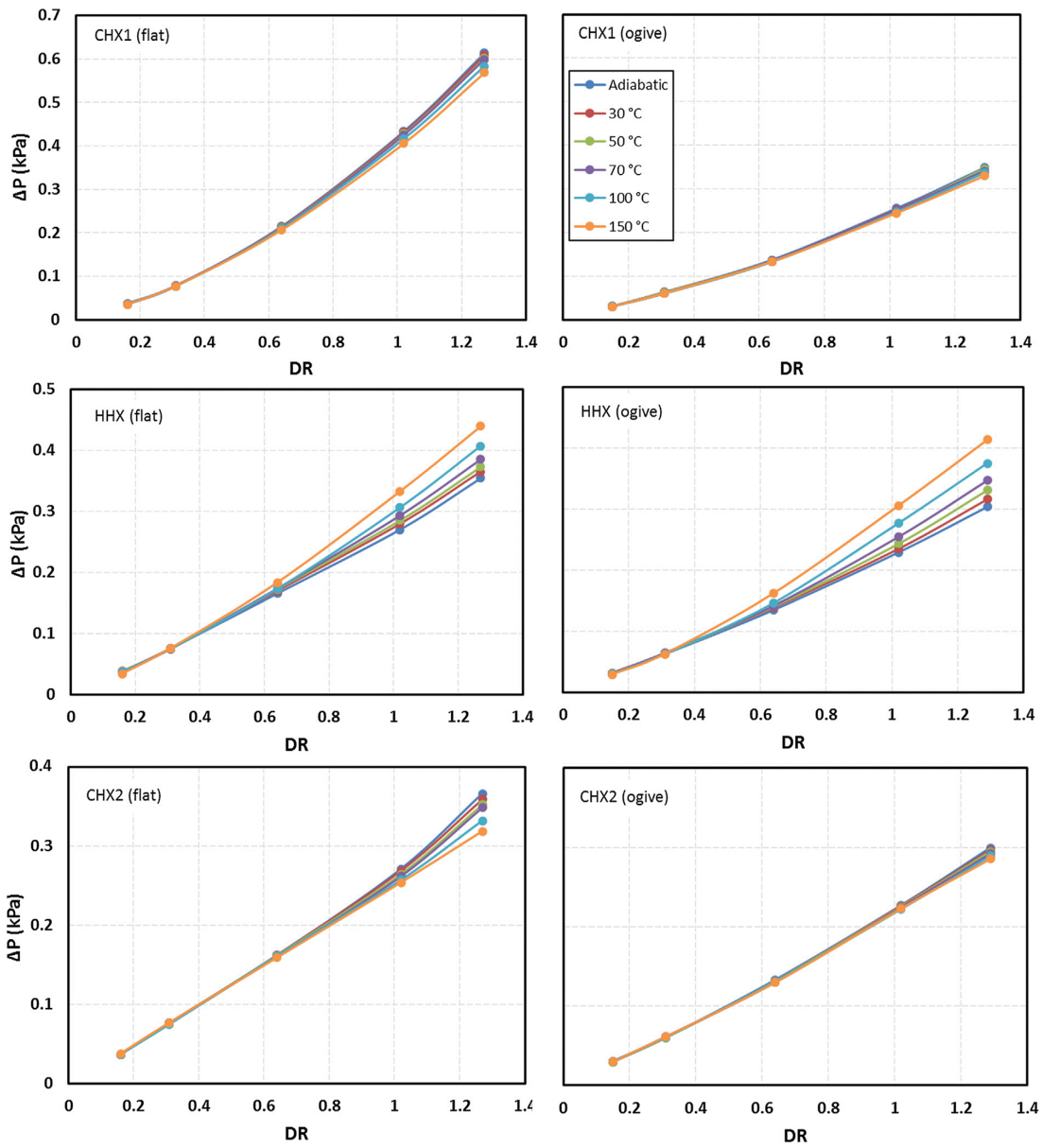
Fig. 16. Comparison between the predicted pressure drop across T-HEX (flat) and T-HEX (ogive).